Polymer Testing 120 (2023) 107953

Contents lists available at ScienceDirect

Polymer Testing

journal homepage: www.elsevier.com/locate/polytest

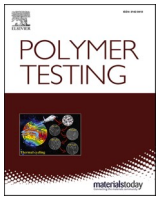

Modal response of hybrid raster orientation on material extrusion printed acrylonitrile butadiene styrene and polyethylene terephthalate glycol under thermo-mechanical loads

Mohammed Dukhi Almutairi [a,b,*], Taheer A. Mascarenhas [a,**], Sultan Saleh Alnahdi [a,c], Feiyang He [a,b], Muhammad A. Khan [a,b,***]

[a] School of Aerospace, Transport, and Manufacturing, Cranfield University, Cranfield, MK43 0AL, UK
[b] Centre for Life-Cycle Engineering and Management, Cranfield University, College Road, Cranfield, MK43 0AL, UK
[c] Sustainable Manufacturing Systems Centre, UK

ARTICLE INFO

Keywords:
Hybrid raster orientation
ABS
PETG
Fatigue bending test
Variable ambient temperature

ABSTRACT

In this paper we look at Acrylonitrile Butadiene Styrene (ABS) and Polyethylene Terephthalate Glycol (PETG), chosen for their low cost, high strength and temperature resistance. This study evaluates the bending fatigue performance of Material extrusion (MEX) ABS and PETG cantilever beams and compares their properties while varying a printing parameter under thermal loads. The study, using custom building orientation angles of 90°, 45° and 60° between the layers, tested the beams at different temperatures from 30° to 50 °C. The results show the effects of the building orientations and the effects of temperature on the sample. The printing orientation, which is the same as loading, also slows the crack growth.

1. Introduction

Three-dimensional printing (3d printing) is a type of manufacturing process by which a three-dimensional object is fabricated from a CAD model or a digital 3d Model [1]. It achieves this by using various processes which deposit or solidify the material using a computer-generated code. Typically, they do this layer by layer, using such materials as plastic filaments, resins and power grains which are fused together [2].

Since its inception in the 1980s this method of manufacturing has been used only to produce prototype parts. At first, using additive manufacturing to produce parts was referred to as Rapid Prototyping. However, due to the advances made in materials, software and precision, additive manufacturing is now being used for industrial production and has become synonymous with 3D Printing. 3D Printing allows the operator to manufacture complex parts and geometric structures which would be impossible for any hand operated machine to craft. 3d printed parts can be hollow or have internal truss structures that help reduce weight [3–5].

A wide array of materials can be 3d printed using various processes. Metal and alloys are generally 3d printed using a powder bed process like Selective Laser Sintering (SLS) or Selective Laser Melting (SLM). Photo Polymers are printed using a Light polymerized process like Stereolithography (SLA), Digital Light Processing (DLP) or Continuous Liquid Interface Production. Thermoplastics are printed using a Material Extrusion (MEX) process. To 3d print a model, one simply selects a CAD file and uploads it into a software app called a slicer. The slicer then creates a g-code which can be fed into the 3d printer [6–9].

Due to its efficiency, low cost and ease of operation, MEX printing is now one of the most widely used process for low volume production and additive manufacturing and is widely used in the automotive, aerospace, biomedical and robotics industries, etc. Fused deposition modelling (FDM), as a material extrusion (MEX) technology defined by ISO/ASTM 52900 [10], is also covered. It employs a heated nozzle to melt raw material filament into a semi-liquid state and then extrudes material layer by layer from the nozzle to print the entire structure [11]. Some of the main polymers used in MEX printing are Polylactic acid (PLA), Acrylonitrile butadiene styrene (ABS), Polyethylene Terephthalate Glycol (PET-G) and Polycarbonate (PC), etc. ABS is one of the most often

* Corresponding author. School of Aerospace, Transport, and Manufacturing, Cranfield University, Cranfield, MK43 0AL, UK.
** Corresponding author.
*** Corresponding author. Centre for Life-Cycle Engineering and Management, Cranfield University, College Road, Cranfield, MK43 0AL, UK.
E-mail addresses: m.almutairi@cranfield.ac.uk (M.D. Almutairi), taheermascarenhas@gmail.com (T.A. Mascarenhas), s.alnahdi@cranfield.ac.uk (S.S. Alnahdi), Feiyang.he@cranfield.ac.uk (F. He), muhammad.a.khan@cranfield.ac.uk (M.A. Khan).

https://doi.org/10.1016/j.polymertesting.2023.107953
Received 25 November 2022; Received in revised form 23 January 2023; Accepted 2 February 2023
Available online 3 February 2023

used thermoplastics, due to its low price, heat resistance and high strength [12].

Various studies carried out discuss the differences in mechanical properties between FDM and conventionally manufactured ABS [13–18]. So far, the hypothesis that most papers point to is that FDM manufactured ABS has 11%–37% less modulus and 22%–57% reduced strength [19,20]. Other studies have assessed the effects of different printing parameters on the mechanical properties of MEX polymers; some have even tried to improve the mechanical properties of the polymer by optimising the printing parameters, but very few studies have focused on the behaviour of MEX ABS under dynamic conditions (fatigue behaviour) because most of the tests that have been conducted are static, with critical parameters relating to the fatigue performance of an MEX part, as shown in Fig. 1 [20–27].

Cracks propagate as a result of repetitive or cyclic loads and failure due to fatigue is normal in structures even where the cyclic stresses are significantly less than the yielding strength. Therefore, it is useful to evaluate the fatigue performance of the materials used. Safai et al., Shanmugam et al., He et al. and Feiyang et al. have reviewed the fatigue behaviour of various MEX polymers [11,28–31]. Their results show that determining the optimal printing parameters is a challenge because the multiple variables in these parameters need to be controlled. It is reported that the building orientation of 45^{o} has the greatest fatigue strength for PLA in tension, but during compact tension tests the 0^{o} and 90^{o} survive fatigue better. According to Letcher and Waytashek and Afrose et al. [32,33], the 45^{o} building orientation produced the highest fatigue strength for 3D-printed polylactic acid (PLA) in tension fatigue tests. The outcomes of a tension fatigue test for FDM ABS were the same [34]. In a compact tension test for FDM PLA, the 0° (X)/90° (Y) raster orientation had the longest fatigue life [35]. In a stress fatigue test, the X orientation of MEX ABS showed the highest fatigue strength [36]. For other printing parameters, several studies conducted flexural fatigue testing for MEX PLA bars, with the findings indicating that increasing layer thickness and nozzle size increased the fatigue life [37,38]. Nonetheless, a comparable study has not been conducted on MEX ABS and PETG.

Most research focuses its attention mainly on mechanical behaviour when printed parts are subjected to static loads, but since the material could fail due to fatigue loadings, it is interesting to understand the influence of the parameters mentioned [11,30,39–43] above on the service life of elements made of 3D printed polymers. Fatigue can occur in the structural components due to cyclical stresses, which leads to catastrophic damage to a lower level of mechanical stresses than normal static load. Besides the process parameters are of interest the mechanical factors characteristic of the fatigue test such as stress amplitude, strain, mean stress, cycle asymmetry coefficient, specific stress–strain ratio, frequency of the stress cycle, self-heating, stress concentrators, etc. Furthermore, some research focused on the strain rate sensitivity of five distinct thermoplastic polymeric materials widely used in AM FFF technology has been thoroughly investigated; for example, ABS and PETG demonstrated low strain rate sensitivity in 3D FFF printing [45]. The strain rate sensitivity index "m" and estimates of toughness for ABS and PETG can tell us more about what mechanical properties we can expect from each polymer under different static tensile loading conditions. Also, the influence of filler inclusion in the polymer matrix on the thermomechanical characteristics of formed composites was also investigated. PET-G was formulated with titanium dioxide, and carbon black was combined with PLA. All measurements were conducted on printed specimens generated using FDM, one of the three-dimensional printing techniques. The addition of TiO2 converted PET-G from a ductile to a brittle material, as the elongation at break decreased four-fold for both filling ratios. The composites' hardness was moderately influenced and decreased with filling [46,47].

Feiyang et al. used ABS and ran their sample under a thermo-mechanical load; they reported that the parts tested on the x orientation 0^{o} were more favourable than the y orientation of 90^{o}. But no-one has yet tried hybrid orientations within the rafters. These are what we tested in the present study. The hybrid orientations used two infill angles when the sample was being printed, for example, 45^{o} and 135^{o} which reveals a 90^{o} spacing between the layers. This experiment focused on testing the effect of various angle offsets on the mechanical properties and the print time.

In this paper chose two critical printing parameters, raster orientation, and layer thickness, and investigated their influence on the crack growth rate of the MEX ABM and PETG cantilever beam under dynamic thermo-mechanical loads. The dynamic bending fatigue test was carried out. Also, the results of this experiment were discussed to determine which hybrid raster orientation withstood most cycles. The results show the effects of the building orientations and the effects of temperature on the sample. The printing orientation, which is the same as loading, also slows the crack growth.

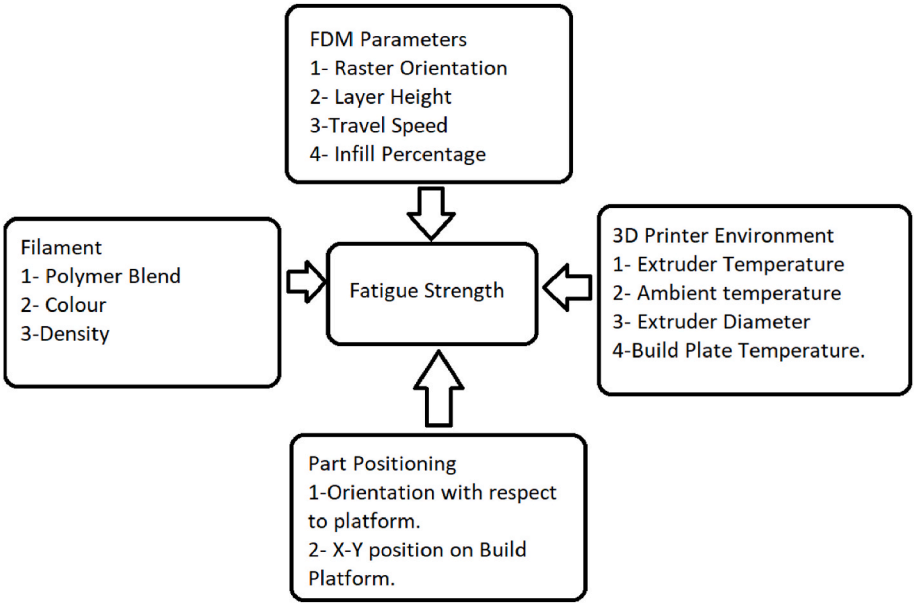

Fig. 1. Critical Parameters relating to the fatigue performance of an MEX part.

2. Methodology

2.1. Design of experiment

The present study focused on three parameters (Nozzle Diameter, Infill Percentage and Layer Height). These are the parameters that affect the quality, manufacturing time and price, as discussed in the introduction. This study also looked at the Raster orientation in the part and showed how varying it affected the strength of the part.

1. Infill Percentage – the strength of the part is directly proportional to the infill percentage; a higher infill percent produces a stronger part.
2. Nozzle Diameter – the nozzle diameter effects the size of the filament extruded: an increase in nozzle diameter results in a quicker print and a smaller diameter result in a more precise print.
3. Layer Thickness – this can also be described as the resolution of the print; it defines the height of each layer and the number of layers per part.
4. Building orientation/Raster Orientation – the building orientation is defined as the path taken by the nozzle to build each layer.

Apart from the nozzle diameter, which must be changed by swapping the nozzle, the remaining parameters are set in the 3d printer's slicer software. Three values, the typical default settings when printing, were assessed for each parameter to span the typical printing parameter range. This allowed for a thorough analysis of the experimental findings. Moreover, the bulging orientation and layer thickness were calculated from the default 3D profile. Not only did these values produce great print quality, but they also covered the average setting range. The selected values for each parameter are shown in in Table 1.

The mechanical properties of ABS and PETG vary when exposed to changes in the environmental temperature; hence, a comparison of fatigue life under different temperatures is significant for research. We intended to look at the effect of three temperatures, 30^{o}, 50 °C and 70 °C. 30 °C was chosen as the bottom limit to simulate equatorial room temperature, but we looked at both 30^{o} and 50 °C. The materials lost some mechanical strength when the temperature rose, making it clear that the structural support would not be strong enough to support the experiment if the ambient temperature rose to 70 °C.

As indicated in Table 1, each printing parameter has three alternatives, resulting in a total of 12 printing parameter combinations. Each combination was put to the test at two different temperatures. Therefore, 36 different specimen types were printed for these parameters and environmental temperature values. Three identical specimens were produced for each combination and evaluated under identical conditions to validate the repeatability of the experimental results.

2.2. Materials

The structures were fabricated by using a (Raise3D pro-2) printer with different types of filaments for (FFF)-based such as ABS has good impact resistance, high rigidity, strain resistance, etc., even at low temperatures, properties that make it a suitable material for the intended application and flexible filaments Polyethylene terephthalate Glycol-Modified (PETG) were selected for their fabric-like properties, such as flexibility and softness, and hence can be a suitable replacement for conventional material. In this study Red ABS and Black PETG from RS PRO were the chosen filaments to make the crack growth and plastic zones easy to observe. More details of these materials are given in Table 2.

Table 1
Printing parameters.

Building Orientations	Nozzle Diameter	Layer Thickness(mm)	Infill %
90°	*0.4*	*0.10*	*100%*
45°			
60°			

2.3. Specimen design

The current standard for testing the flexural fatigue properties of plastics is the ASTM D7774. To achieve this standard, the specimen is loaded cyclically in a positive and a negative direction to a specific stress or strain at a uniform frequency until the specimen ruptures or yields. However, since we were testing 3d printed filaments we put the samples under an additional thermal load. Extra thermo loads and dynamic mechanical loads were applied during the tests. This means the current standard that focuses on the bending fatigue test of polymers may be not suitable in this research. Based on previous research a model of the test sample was made using solid works with the dimensions of 150 mm × 10 mm x 5 mm, as shown in Fig. 2, which is the same as that used in previous research [48]. An initial seed crack was added once the sample had been printed. The model of the specimen was fed into Idea Maker, a g-code slicer with pre-set values for the nozzle diameter of 0.4 mm and a layer thickness of 1 mm. The nozzle and bed temperature were set in accordance with the material used. A crack 1 mm deep was also modelled into the sample.

The specimen's CAD model was converted to an STL file and imported to the Ideal-maker software. Apart from the selected parameters presented in Table 2, there were a series of parameters in Ideal maker. Because these parameters in Ideal maker were not the focus of the current study, all these settings were held at recommended or default values during the printing process. Further, an infill density of 100% was selected. The appropriate set nozzle temperature was selected as 245 °C by ABS and 220 °C for PETG based on the recommendation of the printing setup. The bed temperatures were set to 90 °C for ABS and PETG 60 °C, which was the default value of the printer. Lastly, the Raise3D Pro printer was used to print all the specimens, as shown Fig. 3.

2.4. Specimen batch scheme

To test the prescribed specimen a batch scheme was developed, with each batch receiving three specimens. A total of 12 batches was made using both materials, which would yield a total of 36 samples, 12 samples per orientation. A tabulated list of each batch and their specific orientation can be found in Table 3. The specimen model was converted into an STL file which was then imported into a g-code slicer. Finally, the parameter was set with respect to the batch number and the sample was printed.

2.5. Experimental scheme

The experiment that was conducted was the fatigue bending test. A vibration test was used to evaluate the number of cycles required to fracture the cantilever. A DMA test also was carried out to determine the stiffness of the hybrid raster orientations across both the materials and the storage modulus. The elastic modulus of the beam at different temperatures was determined. The selected values for each parameter were as shown in Fig. 4.

Table 2
Material specifications.

Filament Specifications	ABS	PETG
Diameter	*1.75* mm	*1.75* mm
Tensile Modulus	*2000Mpa*	
Elongation at Yield	*9%*	*20%*
Tensile strength	44 MPa	50 MPa
Melting temperature	*245°C ± 5*	*220°C*
Vicat softening temperature	*103°C*	

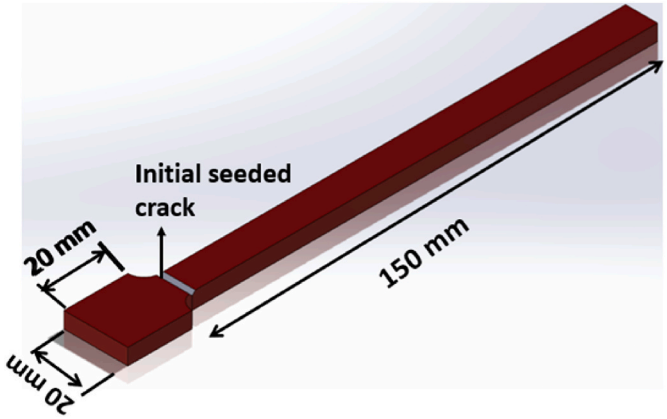

Fig. 2. A picture of the specimen model developed using SolidWorks 2020.

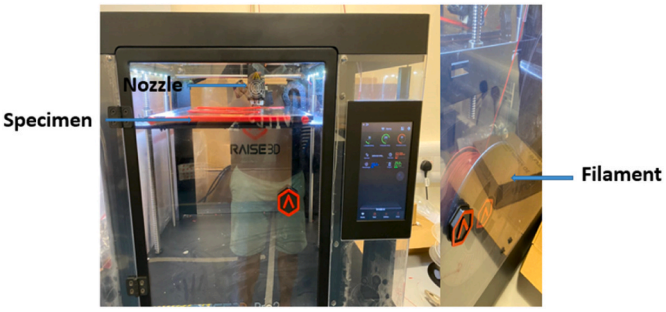

Fig. 3. 3D printing by Raise 3D Pro2.

Table 3
Batch Numbers and their corresponding parameters and test settings.

Batch No.	Orientation Angle	Temperature	Infill Percentage	Material
1	90 (45–135)	30	100%	ABS
2	90 (45–135)	50	100%	ABS
3	45 (45–90)	30	100%	ABS
4	45 (45–90)	50	100%	ABS
5	60 (45–105)	30	100%	ABS
6	60 (45–105)	50	100%	ABS
7	90 (45–135)	30	100%	PETG
8	90 (45–135)	50	100%	PETG
9	45 (45–90)	30	100%	PETG
10	45 (45–90)	50	100%	PETG
11	60 (45–105)	30	100%	PETG
12	60 (45–105)	50	100%	PETG

2.6. Experiment setup and procedure

The first test to be conducted was the bending fatigue test which would subject each batch of specimens to bending fatigue under a thermal load and would record the mean of the cycles to fracture. This was done by connecting the specimen to the V4/T4 shaker manufactured by Data Physics (Hailsham, UK), and a mica heat band was used to provide a constant thermal load. The specimen's natural frequency during the impact test was measured three times with an accelerometer. The sample vibrating under natural frequency provided the initial maximum amplitude of the beam, which significantly shortened the experiment time. Signal Express software was used to record the acceleration and time data from the accelerometer. The signal generator produced a sinusoidal output into the power amplifier. The power amplifier then routed the signal to the shaker, following which the shaker oscillated at a 2 mm amplitude like the natural frequency of the beam. The pre-seeded crack grew until it finally fractured.

Unlike previous studies, the present study directly registered the number of cycles from the beginning of the run to the occurrence of the fracture. Fig. 5, below, shows the experimental setup used for the bending fatigue test. It consisted of a signal generator, DAQ system and Shaker.

The DMA test was then conducted using TA Instruments' Q800 (New Castle, TX, USA). Dual cantilever clamps were used to secure the specimen in the Q800 chamber. The rate of temperature increase was 3.00 °C/min. The oscillation frequency of the load was 1 Hz, was found to be similar to what had been found in other studies [49,50]. This determined the storage modulus of the pieces cut from the previous bending fatigue specimens at temperatures between 30° and 50 °C.

3. Results and discussion

3.1. Dynamic mechanical analysis (DMA) tests

The DMA research on the viscoelastic behaviour of polymer materials includes three evaluations of the storage modulus, which measures the polymeric material's energy storage in the elastic zone. The loss modulus thus indicates the polymer's energy loss in the form of heat [51–56].

To conduct the DMA test, we cut samples from the bending fatigue test and tested them at 30°-50 °C. We tested three samples to make sure of sufficient data and variance. The statistical significance was determined using MATLAB. A Kruskal-Wallis one-way test was conducted with a single independent variable, mainly of raster orientation. This tested the hypothesis that the storage modulus of the different groups of raster orientations of the parameters was equal against the alternative hypothesis that at least one group was different from the others.

The variations for ABS and PETG of the storage modulus according to temperature are presented in, Fig. 6, Figs. 7 and 8 for ABS and PETG. The average storage modulus for various printing parameters is presented in Table 4. Although calculating the mean storage modulus was not the primary objective of the present work, this value can be used as a reference because it has a substantial impact on structural fatigue performance. The higher the storage modulus, the greater the rigidity. It may result in increased life in conditions of fatigue.

the DMA test for ABS and PTEG specimens, the storage modulus constantly decreased as the temperature increased. This is similar to other materials [31,48]. For the average storage modulus under different building orientation printing settings, the building orientation provided the highest value at 90° of the average storage modulus, which is 1290.53 MPa. At 60° orientation, the storage modulus for the sample was only 1255.17 MPa. The mean storage modulus was 1153.75 MPa at 45° building orientation. The fluctuation of the storage modulus was found to be similar to what had been found in other studies [33,57].

The temperature settings on the different building orientations were the same for both ABS and PTEG. ABS had the lowest mean storage modulus at 50 °C, which was 1153.44 MPa. At 30 °C, it provides the mean storage modulus of 1296.18 MPa. However, the nozzle size for all specimens was 0.4 mm, which was found to have a significant effect on the storage modulus.

A statistical study of the data indicated a similar result. The p-value for the 2.18705 x 10–148 building orientation was greater than the p-values for the other printing parameters. It was determined that the storage modulus of MEX, ABS, and PTEG was not greatly affected by variations in building orientation when compared to the other parameters.

3.2. Bending fatigue test

Each group of three samples was subjected to bending fatigue testing, and the average number of cycles to fracture was recorded. Each set's outliers were filtered and removed. The bending fatigue test was carried out at temperatures ranging from 30 °C to 50 °C. Varying results were

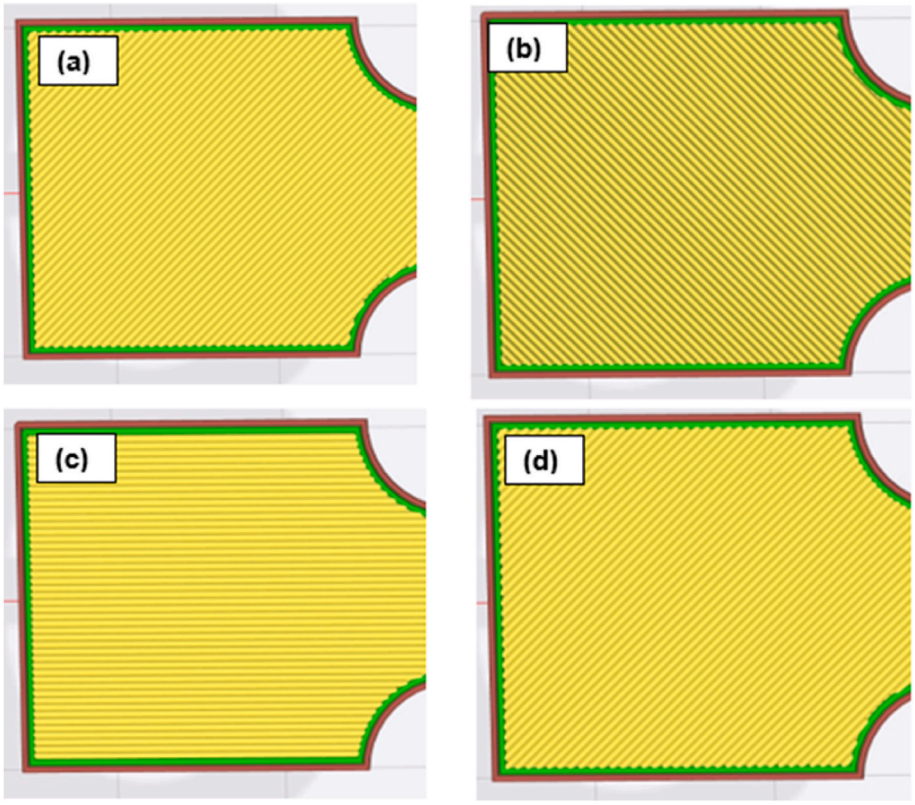

Fig. 4. (a) 45° raster orientation, (b) 135° raster orientation, (c) 90° raster orientation and (d) 105° raster orientation.

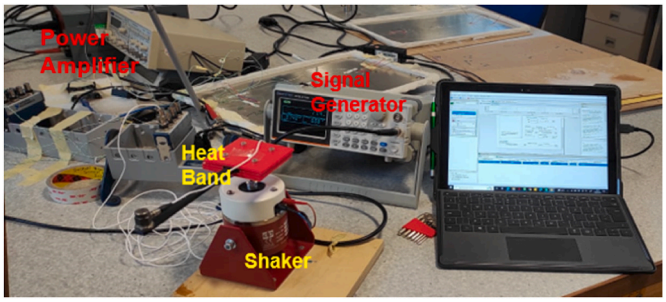

Fig. 5. A picture of the experimental setup.

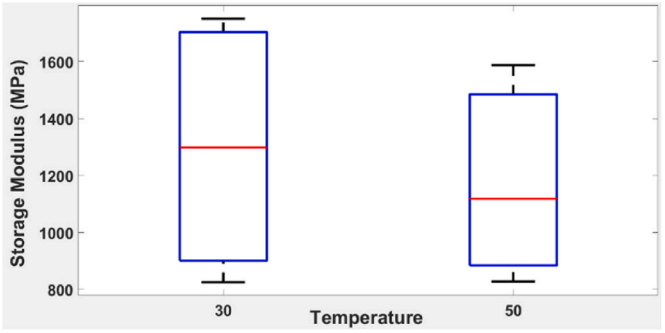

Fig. 6. Detailed storage modulus change for different printing parameters from 30° to 50 °C.

recorded for the hybrid raster orientations; they can be seen below in Table 5 and in the graph in Fig. 9. Fig. 9 demonstrates the average number of cycles to fracture for each parameter combination at various

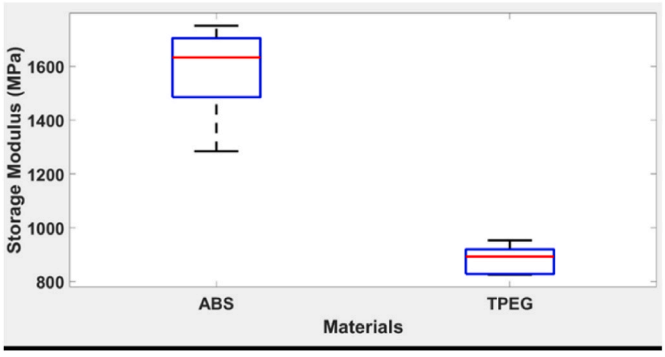

Fig. 7. Alterations in storage modulus for certain ABS and PTEG parameters from 30° to 50 °C.

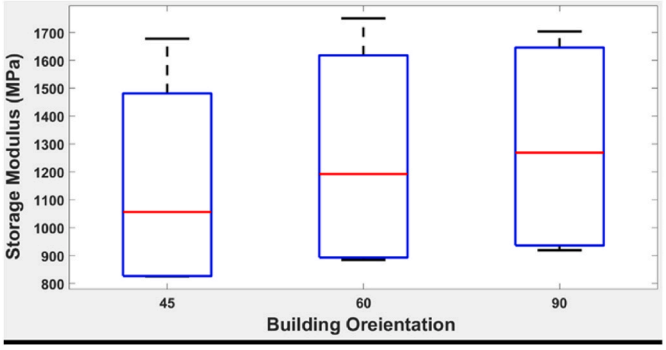

Fig. 8. Statistical analysis of the storage modulus for different building orientations.

Table 4
Mean storage modulus for different printing parameters of ABS and PTEG.

Printing Parameters	Group	Storage Modulus (MPa)	p-Value
Building orientation	*45*	*1153.75*	*4.53281×10^{-110}*
	60	*1255.17*	
	90	*1290.53*	
Temperature	*30*	*1296.18*	*9.25489×10^{-113}*
	50	*1153.44*	
Materials	*ABS*	*1581.36*	*2.18705×10^{-148}*
	PETG	*884.93*	

Table 5
Results of the bending fatigue test for number of cycles and different orientations ignoring other printing parameters.

Raster Orientation	Material	Environmental Temperature	Mean Number of cycles until fracture
90 (45–135) Default	*ABS*	*30°C*	*1879*
		50°C	*1993.5*
	PETG	*30°C*	*1518.5*
		50°C	*1544*
45 (45–90)	*ABS*	*30°C*	*1845.5*
		50°C	*2031.5*
	PETG	*30°C*	*1523.5*
		50°C	*1586.5*
60 (45–105)	*ABS*	*30°C*	*1933.5*
		50°C	*1718*
	PETG	*30°C*	*1580.5*
		50°C	*1692*

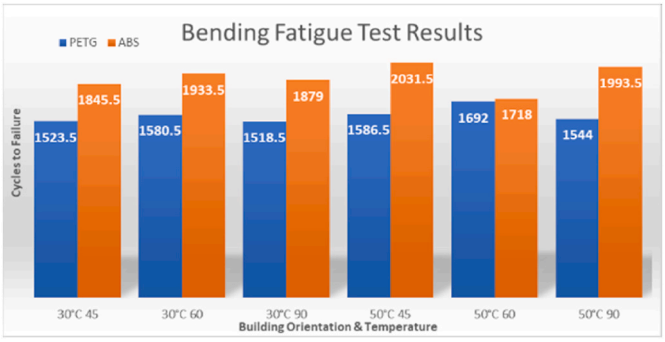

Fig. 9. The results of the bending fatigue test.

environmental temperatures. As can be seen, the specimen with a 45 ABS and 60 PETG raster orientations, printing had the longest fatigue life until the fracture at different environmental temperatures.

3.2.1. Temperature effects on bending fatigue test results

Table 5 shows the variation in the fatigue life in different conditions. The change in ambient temperature significantly affected the specimens fatigue life. Furthermore, the mean number of cycles to the point of fracture had 2032.5 on ABS at 50 °C cycles for the 45 orientations. However, the 90-building orientation had approximately 1518.5 cycles on PTEG at 30 °C. The previous papers examining this effect all show that fatigue resistance decreases with increase in temperature [31,44,47,56–59]. The mean temperature was calculated using the three specimens that were used for each test, increasing the temperature from 30 °C to 50 °C. The increases in the number of cycles are recorded across all variations (see Fig. 10). The reason this may have been that the increase in temperature causes the plastic to behave more elastically.

The most significant effect of temperature on fatigue life was the loss of mechanical properties as the temperature rose. In terms of the molecular microstructure, FFF ABS and PETG exhibited a vitreous appearance at lower temperatures. In other words, the rotation of the molecular chain paused, preventing the coil from uncoiling and elongating [60]. By increasing the environmental temperature, the energy of the moving units and movable space increased. Therefore, it can be concluded that microstructural fractures, crack initiation, and propagation are easier in FFF ABS and PTEG at higher temperatures. Furthermore, such changes in the microstructural properties influence the mechanical behaviour of the specimens. Finally, changes in the microstructure and mechanical behaviour of FFF ABS and PTEG significantly contribute to the fatigue life of the beam. The DMA results presented later in this article support the change in mechanical behaviour.

3.2.2. Raster orientation effects on bending fatigue test results

The raster orientation is a critical parameter that affects the fatigue life of the specimens. At the ambient temperature (30 °C) we saw how the PETG 60 (45–105) default orientation performs better than the rest but at 50 °C we found that the ABS 45 (45–90) orientation performs better. This is reported in Fig. 11 where the 45° is shown to have the highest ratio of cycles to fatigue under at a temperature of 50 °C. One possible reason for the better of this orientation was the lack of microscopic printing defects.

The outcomes are reasonable. On the beam, the initial seeded fracture is lateral, the same as in the case of the specimen with a building orientation of 60°. In fracture mechanics, microcracks on or within the structure begin and propagate the crack [61]. The micro-voids occur between the filaments in the structure due to 3D printing defects in the research. When the beam vibrates, the existence of these air gaps between the fibres causes stress concentration.

Moreover, Moreover, the weakest connections between filaments are seen in places where voids are present. Notably, the orientation of the void region is identical to that of the first crack seed. This results in a good crack route and rapid crack propagation. In contrast, because of the vibration of the beam, the bending force is longitudinal and acts vertically on the 60 orientation voids, hence increasing crack formation and reducing fatigue life.

3.3. Fractography

After the bending fatigue tests, various images of the specimen fracture section were captured using the Dino-Lite digital microscope (AnMo Electronics Corporation, Hsinchu, China). A diagram indicating which cross-section the Dino-Lite digital microscope captured is shown in Fig. 12.

Stress-whitening, a universal occurrence in polymers, is induced by microvoids and crazes [62]. The polymer chains restructure under strain whenever the beam vibrates. In rare instances, the straightening, sliding, and shearing of the fillers and polymer chains during movement within the microenvironment of the plastic may result in the creation of occlusions or holes. When these occlusions merge, they generate microvoids. The microvoids alter the plastic's refractive index, causing the object to appear white.

In Particular, the defects (voids) of the 3D-printed ABS and PETG materials produce localised stress concentration, and these regions are more likely to develop cracks.

Along the crack route of the specimen at 45 building orientation, the inter-filament bonding strength was similarly extremely weak. As shown in Figs. 13 and 14, certain filaments peeled away from the cracked surface.

Furthermore, from the figures mentioned above, it could be observed in all the pictures that the crack growth rate was time dependent. The white and red areas appeared alternately in the direction along which the crack propagated. This meant that crack growth dominated alternately by the ductile break and brittle break was occurring. The layer-by-layer 3D-printed structure may have led to this phenomenon. Furthermore, the brittle break rate in the red area was higher than that of the ductile break in the white area. It was also reflected in the global colour distribution in the direction in which the crack spread in the section. The colour near the beam surface was significantly whiter than

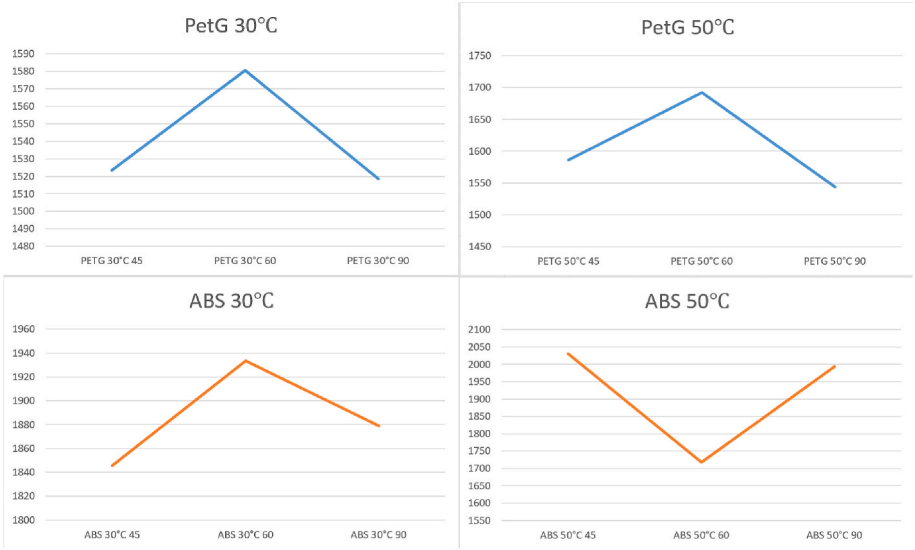

Fig. 10. Effect of temperature on fatigue life.

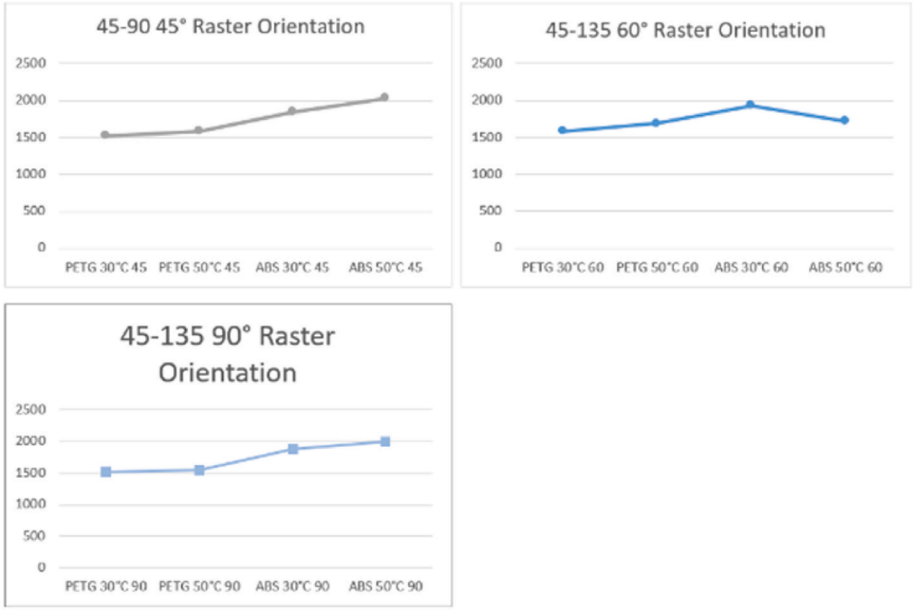

Fig. 11. Building orientation effect on fatigue life.

that in the bottom area. The ductile break gradually changed to a brittle break during the crack propagation. This implied that the initial crack growth rate was less than it became because the stress at the tip of the crack may have increased along with the depth of the crack. The greater the stress, the faster and easier the brittle fracture.

We could observe the printing defects in each raster orientation, called micro voids. These were particularly visible in the default orientation in Fig. 15. The presence of this void made the internal structure much weaker than with the 45° and 60° deflection (Figs. 13 and 14). In Fig. 9 we saw that the 45° orientation performed better than the others; this may be attributed to the lack of defects within the test sample. In this situation, the brittle fracture continued along this section. The voids between each filament and layer, represented by dark red, occupied a large area of the fracture surface, thereby speeding up the crack growth rate.

For the building orientation of the PTEG effect, when Fig. 16 was compared with Fig. 17, we saw that the section with a layer that was 0.10 mm thick had fewer defects (densely black areas) between the layers in the unit section. This may be the reason for its longer fatigue life.

The specimen with a 60-orientation had the lowest crack growth rate for the same stress intensity factor as shown in Figs. 18 and 19. The crack growth rate of the 90-orientation specimen was between that of the 45 and 60 orientation specimens. In contrast, the 60-orientation specimen had the highest crack growth rate. This meant that the 45 orientation specimens had the best fatigue strength, and the 60 orientation specimens had the shortest fatigue life for the same cyclic stress conditions.

The inter-filament bonding strength is also very weak along the crack path of the specimen with a building orientation of 60. As can be seen from Figs. 18 and 19, some loose filaments are peeled off the fractured surface. For the layer thickness effect, we can see that the section with a 0.10 mm layer thickness has fewer defects (densely black area) between the layers in the unit section. This may be the reason why it has a longer fatigue life.

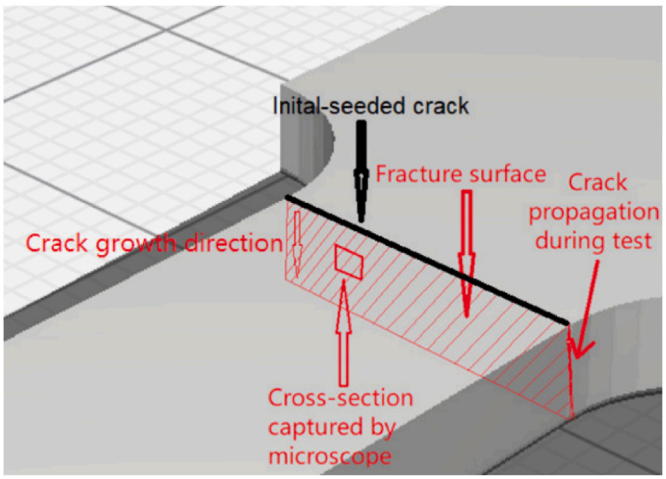

Fig. 12. A diagram *indicating which cross-section the Dino-Lite digital microscope captured from Ref. [31].*

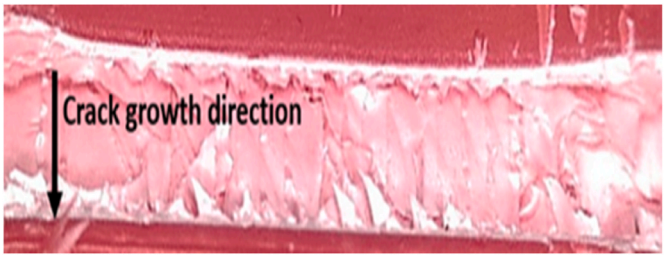

Fig. 13. Specimen with ABS 45–90 45 deflection of nozzle size 0.4 mm.

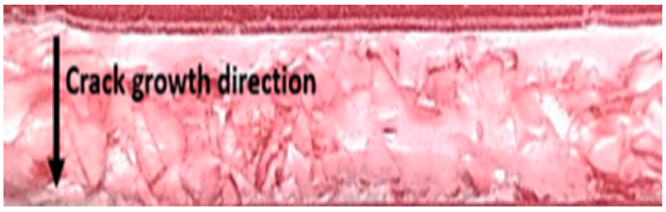

Fig. 14. Specimen at ABS 45–105 60 deflection of nozzle size 0.4 mm.

Fig. 15. Specimen at ABS 45–135 90 orientation of nozzle size 0.4 mm.

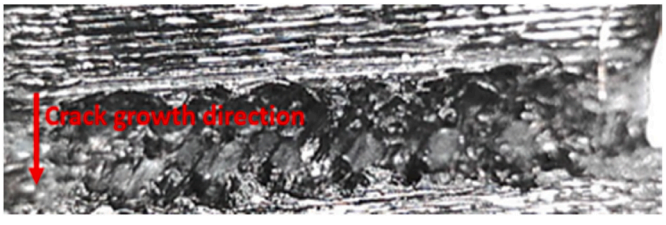

Fig. 16. Specimen PTEG at 45-90-45 (30 °C) orientation of nozzle size 0.4 mm.

Fig. 17. Specimen PTEG at 45-90-45 (50 °C) orientation of nozzle size 0.4 mm.

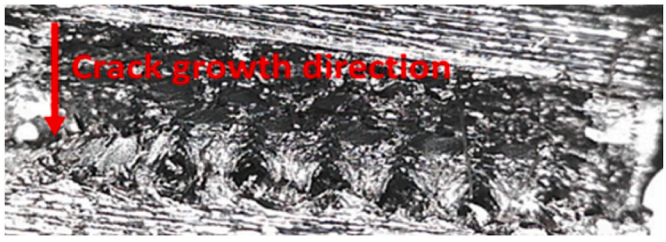

Fig. 18. Specimen at PETG 45–105 60 (30 °C) orientation of nozzle size 0.4 mm.

Fig. 19. Specimen at PETG 45–105 60 (50 °C) orientation of nozzle size 0.4 mm.

4. Conclusion

After investigating the influence of a Printing Parameter (Raster Orientation) and environmental temperature on the bending fatigue of PETG and ABS, we were able to draw the following conclusion.

1. The change in ambient temperature has great impact on the fatigue life of the samples, as shown in the results (see Table 4).
2. At the ambient room temperature PETG outperforms ABS; hence, we can conclude that it is better to deal with PETG parts at room temperature using the default setting.
3. At 50 °C ABS 45–90 works better than any other combination of raster orientation. This can therefore be recommended as a printing parameter when producing parts that will face thermal load.
4. These results are trustworthy given the type of material and the influence of the environmental temperature on crack growth.
5. Preliminary experimental results showed that the specimens in 45 orientation have the lowest crack growth rates.
6. The mechanical properties of ABS and PETG specimens fabricated by fused deposition modelling display are significantly influenced not only by the infill rates as expected, but also about the printed pattern of different layers and their orientation. Even some specimens were printed with a setting of 100% infill, the actual positive or negative air gaps should be determined or estimated more accurate.

In this paper we can conclude the for parts are to be used at room temperature PETG is better than ABS. The analytical modelling of the relationship between these printing parameters and the bending fatigue life of the ABS and PTEG beams is to be expanded in a future study.

Declaration of competing interest

The authors declare the following financial interests/personal relationships which may be considered as potential competing interests: Student at Cranfield university.

Data availability

Data will be made available on request.

References

[1] 3D printing scales up, Economist (5 September 2013). https://www.economist.com/technology-quarterly/2013/09/05/3d-printing-scales-up. Accessed on 21-09-2022.

[2] Jon Excell, The engineer, in: The Rise of Additive Manufacturing, 23 May 2010. Retrieved 30 October 2013.

[3] Learning Course: Additive Manufacturing – Additive Fertigung". tmg-muenchen.de.

[4] Hugo K.S. Lam, Li Ding, T.C.E. Cheng, Honggeng Zhou, The impact of 3D printing implementation on stock returns: a contingent dynamic capabilities perspective, Int. J. Oper. Prod. Manag. 39 (6/7/8) (2019) 935–961, https://doi.org/10.1108/IJOPM-01-2019-0075. ISSN 0144-3577. S2CID 211386031.

[5] Jump up To:[a] [B] "Most Used 3D Printing Technologies 2017–2018 | Statistic". Statista. Retrieved 2 December 2018.

[6] Jane Bird, Exploring the 3D Printing Opportunity, The Financial Times, 2012-08-08. Retrieved 2012-08-30.

[7] Hairul Hisham Hamzah, Saiful Arifin Shafiee, Aya Abdalla, Bhavik Anil Patel, 3D printable conductive materials for the fabrication of electrochemical sensors: a mini review, Electrochem. Commun. 96 (2018) 27–31, https://doi.org/10.1016/j.elecom.2018.09.006. S2CID 105586826.

[8] FDM Is a Proprietary Term Owned by Stratasys. All 3-D Printers that Are Not Stratasys Machines and Use a Fused Filament Process Are Referred to as or Fused Filament Fabrication (FFF).

[9] A. Anderson. "A Whole New Dimension: Rich Homes Can Afford 3D Printers," The Economist, 15th November 2007 Retrieved from http://www.economist.com/node/10105016?story_id=10105016 25.11.2022.

[10] ISO/TC 261, Additive Manufacturing ISO/ASTM 52900:2021 (En), Additive Manufacturing—General Principles—Fundamentals and Vocabulary, ISO, Geneva, Switzerland, 2021.

[11] V. Shanmugam, O. Das, K. Babu, U. Marimuthu, A. Veerasimman, D.J. Johnson, R. E. Neisiany, M.S. Hedenqvist, S. Ramakrishna, F. Berto, Fatigue behaviour of FDM-3D printed polymers, polymeric composites and architected cellular materials, Int. J. Fatig. 143 (2021), 106007 ([CrossRef]).

[12] A.M. Peterson, Review of acrylonitrile butadiene styrene in fused filament fabrication: a plastics engineering-focused perspective, Addit. Manuf. 27 (2019) 363–371 ([CrossRef]).

[13] C. Ziemian, M. Sharma, S. Ziemi, Anisotropic mechanical properties of ABS parts fabricated by fused deposition modelling, in: M. Gokcek (Ed.), Mechanical Engineering, IntechOpen Limited, London, 2012.

[14] A.R. Torrado, C.M. Shemelya, J.D. English, Y. Lin, R.B. Wicker, D.A. Roberson, Characterizing the effect of additives to ABS on the mechanical property anisotropy of specimens fabricated by material extrusion 3D printing, Addit. Manuf. 6 (2015) 16–29 ([CrossRef]).

[15] S. Ahn, M. Montero, D. Odell, S. Roundy, P.K. Wright, M. Montero, P.K. Wright, Anisotropic material properties of fused deposition modeling ABS, Rapid Prototyp. J. 8 (2002) 248–257 ([CrossRef]).

[16] B.H. Lee, J. Abdullah, Z.A. Khan, Optimization of rapid prototyping parameters for production of flexible ABS object, J. Mater. Process. Technol. 169 (2005) 54–61 ([CrossRef]).

[17] K. Hibbert, G. Warner, C. Brown, O. Ajide, G. Owolabi, A. Azimi, The effects of build parameters and strain rate on the mechanical properties of FDM 3D-printed acrylonitrile butadiene styrene, Open J. Org. Polym. Mater. 9 (2019) 1–27 ([CrossRef]).

[18] B.M. Tymrak, M. Kreiger, J.M. Pearce, Mechanical properties of components fabricated with open-source 3-D printers under realistic environmental conditions, Mater. Des. 58 (2014) 242–246 ([CrossRef]).

[19] J.F. Rodriguez, J.P. Thomas, J. Renaud, Mechanical behavior of acrylonitrile butadiene styrene (ABS) fused deposition materials, Experimental investigation. Rapid Prototyp. J. 7 (2001) 148–158 ([CrossRef]).

[20] J.F. Rodríguez, J.P. Thomas, J.E. Renaud, Mechanical behavior of acrylonitrile butadiene styrene fused deposition materials modelling, Rapid Prototyp. J. 9 (2003) 219–230 ([CrossRef]).

[21] C. Bellehumeur, L. Li, Q. Sun, P. Gu, Modeling of bond formation between polymer filaments in the fused deposition modeling process, J. Manuf. Process. 6 (2004) 170–178 ([CrossRef]).

[22] A.C. Abbott, G.P. Tandon, R.L. Bradford, H. Koerner, J.W. Baur, Process-structure-property effects on ABS bond strength in fused filament fabrication, Addit. Manuf. 19 (2018) 29–38 ([CrossRef]).

[23] M.S. Chaudhry, A. Czekanski, Evaluating FDM process parameter sensitive mechanical performance of elastomers at various strain rates of loading, Materials 13 (2020) 3202 ([CrossRef]).

[24] N.S.F. Jap, G.M. Pearce, A.K. Hellier, N. Russell, W.C. Parr, W.R. Walsh, The effect of raster orientation on the static and fatigue properties of filament deposited ABS polymer, Int. J. Fatig. 124 (2019) 328–337 ([CrossRef]).

[25] C.W. Ziemian, R.D. Ziemian, K.V. Haile, Characterization of stiffness degradation caused by fatigue damage of additive manufactured parts, Mater. Des. 109 (2016) 209–218 ([CrossRef]).

[26] S. Ziemian, M. Okwara, C.W. Ziemian, Tensile and fatigue behavior of layered acrylonitrile butadiene styrene, Rapid Prototyp. J. 21 (2015) 270–278 ([CrossRef]).

[27] K.R. Hart, E.D. Wetzel, Fracture behavior of additively manufactured acrylonitrile butadiene styrene (ABS) materials, Eng. Fract. Mech. 177 (2017) 1–13 ([CrossRef]).

[28] M.M. Padzi, M.M. Bazin, W.M.W. Muhamad, Fatigue characteristics of 3D printed acrylonitrile butadiene styrene (ABS), IOP Conf. Ser. Mater. Sci. Eng. 269 (2017), 012060 ([CrossRef]).

[29] F. He, V. Kumar, M.A. Khan, Evolution and new horizons in modelling crack mechanics of polymeric structures, Mater. Today Chem. 20 (2020), 100393.

[30] L. Safai, J.S. Cuellar, G. Smit, A.A. Zadpoor, A review of the fatigue behavior of 3D printed polymers, Addit. Manuf. 28 (2019) 87–97 ([CrossRef]).

[31] F. He, M. Khan, Effects of printing parameters on the fatigue behaviour of 3D-printed ABS under dynamic thermo-mechanical loads, Polymers 13 (2021) 2362, https://doi.org/10.3390/polym13142362.

[32] T. Letcher, M. Waytashek, Material property testing of 3D-printed specimen in pla on an entry-level 3D printer, in: Proceedings of the ASME International Mechanical Engineering Congress and Exposition, Proceedings (IMECE), Montreal, QC, Canada 2A, 2014.

[33] M.F. Afrose, S.H. Masood, P. Iovenitti, M. Nikzad, I. Sbarski, Effects of part build orientations on fatigue behaviour of FDM-processed PLA material, Prog. Addit. Manuf. 1 (2016) 21–28.

[34] C.W. Ziemian, R.D. Ziemian, K.V. Haile, Characterization of stiffness degradation caused by fatigue damage of additive manufactured parts, Mater. Des. 109 (2016) 209–218.

[35] F. Arbeiter, M. Spoerk, J. Wiener, A. Gosch, G. Pinter, Fracture mechanical characterization and lifetime estimation of near- homogeneous components produced by fused filament fabrication, Polym. Test. 66 (2018) 105–113.

[36] N. Lokesh, B.A. Praveena, J.S. Reddy, V.K. Vasu, S. Vijaykumar, Evaluation on effect of printing process parameter through Taguchi approach on mechanical properties of 3D printed PLA specimens using FDM at constant printing temperature, Mater. Today Proc. 52 (2022) 1288–1293.

[37] M. Azadi, A. Dadashi, M. Sadegh Aghareb Parast, S. Dezianian, A. Bagheri, A. Kami, V. Asghari, A comparative study for high-cycle bending fatigue lifetime and fracture behavior of extruded and additive-manufactured 3D-printed acrylonitrile butadiene styrene polymers, Int J Addit Manufact Struct 1 (1) (2022) 1.

[38] F. He, H. Ning, M. Khan, Effect of 3D printing process parameters on damping characteristic of cantilever beams fabricated using material extrusion, Polymers 15 (2) (2023) 257.

[39] N.S. Jap, G.M. Pearce, A.K. Hellier, N. Russell, W.C. Parr, W.R. Walsh, The effect of raster orientation on the static and fatigue properties of filament deposited ABS polymer, Int. J. Fatig. 124 (2019) 328–337.

[40] O.H. Ezeh, L. Susmel, Fatigue strength of additively manufactured polylactide (PLA): effect of raster angle and non-zero mean stresses, Int. J. Fatig. 126 (2019) 319–326.

[41] R. Jerez-Mesa, J.A. Travieso-Rodriguez, J. Llumà-Fuentes, G. Gomez-Gras, D. Puig, Fatigue lifespan study of PLA parts obtained by additive manufacturing, Procedia Manuf. 13 (2017) 872–879.

[42] J.M. Puigoriol-Forcada, A. Alsina, A.G. Salazar-Martín, G. Gomez-Gras, M.A. Pérez, Flexural fatigue properties of polycarbonate fused-deposition modelling specimens, Mater. Des. 155 (2018) 414–421.

[43] M.C. Dudescu, L. Racz, F. Popa, Effect of infill pattern on fatigue characteristics of 3D printed polymers, Materials Today: Proceedings (2022).

[44] A. Mura, A. Ricci, G. Canavese, Investigation of fatigue behavior of ABS and PC-ABS polymers at different temperatures, Materials 11 (2018) 1818 ([CrossRef]).

[45] N. Vidakis, M. Petousis, E. Velidakis, M. Liebscher, V. Mechtcherine, L. Tzounis, On the strain rate sensitivity of fused filament fabrication (Fff) processed pla, abs, petg, pa6, and pp thermoplastic polymers, Polymers 12 (12) (2020) 2924.

[46] D. Froš, P. Veselý, Thermomechanical assessment of novel composites intended for fused deposition modeling, in: 2022 45th International Spring Seminar on Electronics Technology (ISSE), IEEE, 2022, May, pp. 1–8.

[47] H.S. Kim, X.M. Wang, N.A.H.N. Abdullah, Effect of temperature on fatigue crack growth in the polymer abs, Fatig. Fract. Eng. Mater. Struct. 17 (1994) 361–367 ([CrossRef]).

[48] H. Baqasah, F. He, B.A. Zai, M. Asif, K.A. Khan, V.K. Thakur, M.A. Khan, In-situ dynamic response measurement for damage quantification of 3D printed ABS cantilever beam under thermomechanical load, Polymers 11 (2019) 2079.

[49] S.U. Zhang, J. Han, H.W. Kang, Temperature-dependent mechanical properties of ABS parts fabricated by fused deposition modeling and vapor smoothing, Int. J. Precis. Eng. Manuf. 18 (5) (2017) 763–769.

[50] Z. Weng, J. Wang, T. Senthil, L. Wu, Mechanical and thermal properties of ABS/montmorillonite nanocomposites for fused deposition modeling 3D printing, Mater. Des. 102 (2016) 276–283.

[51] N. Vidakis, M. Petousis, E. Velidakis, N. Mountakis, P.E. Fischer-Griffiths, S. Grammatikos, L. Tzounis, Fused filament fabrication three-dimensional printing multi-Functional of polylactic acid/carbon black nanocomposites, Chimia 7 (3) (2021) 52.

[52] M. Petousis, N. Vidakis, N. Mountakis, S. Grammatikos, V. Papadakis, C.N. David, S.C. Das, Silicon carbide nanoparticles as a mechanical boosting agent in material extrusion 3D-printed polycarbonate, Polymers 14 (17) (2022) 3492.
[53] K. Arunprasath, M. Vijayakumar, M. Ramarao, T.G. Arul, S.P. Pauldoss, M. Selwin, V. Manikandan, Dynamic mechanical analysis performance of pure 3D printed polylactic acid (PLA) and acrylonitrile butadiene styrene (ABS), Mater. Today Proc. 50 (2022) 1559–1562.
[54] N. Vidakis, M. Petousis, S. Grammatikos, V. Papadakis, A. Korlos, N. Mountakis, High performance polycarbonate nanocomposites mechanically boosted with titanium carbide in material extrusion additive manufacturing, Nanomaterials 12 (7) (2022) 1068.
[55] N. Vidakis, M. Petousis, N. Mountakis, S. Grammatikos, V. Papadakis, J. D. Kechagias, S.C. Das, On the thermal and mechanical performance of polycarbonate/titanium nitride nanocomposites in material extrusion additive manufacturing, Composites Part C: Open Access 8 (2022), 100291.
[56] A. Arivazhagan, S.H. Masood, Dynamic mechanical properties of ABS material processed by fused deposition modelling, Int. J. Eng. Res. Afr. 2 (3) (2012) 2009–2014.
[57] H.O.S. Kim, X.M. Wang, Temperature and frequency effects on fatigue crack growth in acrylonitrile-butadiene-styrene (ABS), J. Appl. Polym. Sci. 57 (1995) 811–817 ([CrossRef]).
[58] B. Rankouhi, S. Javadpour, F. Delfanian, T. Letcher, Failure analysis and mechanical characterization of 3D printed ABS with respect to layer thickness and orientation, J. Fail. Anal. Prev. 16 (2016) 467–481.
[59] M.D. Almutairi, S.S. Alnahdi, M.A. Khan, Strain release behaviour during crack growth of a polymeric beam under elastic loads for self-healing, Polymers 14 (15) (2022). Article No. 3102.
[60] Introduction to polymers, Available online: https://www.open.edu/openlearn/science-maths-technology/science/chemistry/introduction-polymers/content-section-2.5.3. (Accessed 26 December 2022).
[61] C.H. Wang, Introduction to Fracture Mechanics, DSTO Aeronautical and Maritime Research Laboratory, Kensington, NSW, Australia, 1996.
[62] C.B. Bucknall, R.R. Smith, Stress-whitening in high-impact polystyrenes, Polymer 6 (8) (1965) 437–446.